Investigating the vapour phase synthesis of copper terephthalate metal organic framework thin films by atomic/molecular layer deposition

Ben Gikonyo, Fangbing Liu, Siddhartha De, Catherine Journet, Catherine Marichy, Alexandra Fateeva

Investigating the vapour phase synthesis of copper terephthalate Metal Organic Framework thin films by atomic/molecular layer deposition

Ben Gikonyo, Fangbing Liu, Siddhartha De, Catherine Journet, Catherine Marichy,* and Alexandra Fateeva,*

Laboratoire des Multimatériaux et Interfaces, UMR CNRS 5615, Univ. Lyon, Université Claude Bernard Lyon 1, F-69622 Villeurbanne, France

ABSTRACT

Solventless synthesis and processing of Metal Organic Frameworks (MOFs) is critical to implement these materials in applied technologies. Vapour phase synthesis of MOF thin films is particularly suitable for such applications, but challenging compared to the conventional solution based methods. It is therefore compelling to advance and widen the vapour phase synthesis of MOF thin films. Crystalline copper terephthalate MOF thin films are grown in vapour phase by the means of atomic and molecular layer deposition (ALD/MLD) on different kinds of substrates. Expanding from the pioneer work, the formation of the 3D phase is clearly evidenced for the first time and the adaptability of the process to several kinds of substrates is revealed. A directional film growth is observed at the early stage of the ALD/MLD process leading to oriented MOF crystallites on a surface, when isotropical growth proceeds with the increasing number of ALD/MLD cycles. Notably, this study primary demonstrates a heteroepitaxial growth achievable in the vapour phase by using DMOF-1 single crystals as the starting surface with a lattice matching topology. Such approach offers an appealing pathway to develop MOF on MOF superlattice materials in vapour phase.

Keywords: MOF, thin films, vapour phase synthesis, hybrid materials, atomic layer deposition, molecular layer deposition, epitaxy.

1. Introduction

Atomic layer deposition (ALD) is a classical thin film growth technique mainly applied to the microelectronics industry[1–4]. It is based on successive self-limited reactions between gas phase precursors and a solid surface, allowing to grow a film layer by layer with an atomic scale control of the thickness[5,6]. Though ALD is mostly used for the synthesis of inorganic materials, noticeable progress was made when the molecular layer deposition (MLD) of organic polymers was first reported in the 1990's[7], followed by the growth of hybrid materials in 2008[8]. The adaptability of this technique to the growth of materials using precursors that could lead to MOF was first demonstrated in 2010 by Klepper et al. who reported an ALD/MLD process of several aluminium carboxylates, although the resulting films were amorphous[9]. Hence, a major breakthrough for the vapour phase synthesis of crystalline MOF thin films via ALD/MLD was performed in 2016 by Ahvenniemi et al. who reported the direct growth of crystalline copper terephthalate (CuTPA)[10].

Since this seminal study, the great majority of ALD/MLD of crystalline MOFs is reported by the group of Karppinen in Alto University[11–16]. In other cases, MOF thin films were obtained in two steps as after the ALD/MLD process, a vapour post-treatment was necessary to achieve a crystalline film[17–21]. This later approach is less desirable, as it somehow cancels the great advantage of all-gas phase processing. Indeed, vapour phase synthesis of MOFs thin films is a highly attractive strategy when contemplating MOF integration into devices[22–24]. In conjunction with reducing environmental impact, solvents should be avoided for device fabrication regarding the contamination and corrosion risks[25] as well as the generated surface tension during evaporation[26]. Moreover, when considering MOF chemistry, developing the vapour film growth opens

great opportunity in terms of achieving superlattice structures that are especially challenging with equilibrated solution-based reactions.
Therefore, ALD/MLD growth of MOF thin films represents a unique opportunity both at the fundamental level and for industrial applications. This promising technique is for now however restricted in terms of scientific groups worldwide, methods, and materials. To develop and investigate the ALD/MLD of MOFs we focused on the first reported crystalline material: CuTPA[10]. In this reference work, the authors demonstrated that the film thickness was linear to the number of cycles, with a growth per cycle (GPC) of 3 Å at 180 °C. Grazing Incidence X-Ray Diffraction (GIXRD) data were recorded and a 2D paddle-wheel MOF-2 structure was deduced, although the experimental data were not compared against the corresponding calculated XRD diagram. No morphological characterizations by the means of electron microscopy were provided, precluding the appreciation of the surface coverage, homogeneity, and the crystals topology. Here, we present thorough characterisations of the film structure, clarify the phase identification, and inspect the morphology of the crystalline MOF films. More importantly, we extend the process by investigating the film growth on different kinds of substrates. Beyond the MOF deposition on oxide substrates, we demonstrate for the first time a heteroepitaxial MOF on MOF growth in vapour phase using DMOF-1 single crystal as the substrate and leading to an unprecedented heterostructure.

2. Materials and methods

A home-made manual ALD/MLD reactor was developed (see supporting information for the details, section C and Figure S9), with pressure and temperature control over the precursor cylinders and the deposition chamber. Terephthalic acid (TPA) and copper 2,2,6,6-tetramethyl-3,5-heptanedione Cu(thd)$_2$ were used as reactants according to the reported procedure[10], and were kept at 180 and 110 °C, respectively. Ahvenniemi et al. reported the growth of crystalline CuTPA films between 180 °C and 195 °C, and of amorphous layers above 195 °C [10]. As no noticeable change was observed within this range, the reaction chamber temperature was set to 190 °C. Depositions were performed at a pressure of 2 mbar, using Argon as a carrier gas. First tests were performed on Si (100) substrates with the native oxide, then MOF films were grown on FTO, sapphire and DMOF-1 single crystal. The synthesis procedures and characterizations of the bulk MOF sample (Figures S3, S4 and S5), DMOF-1 single crystals (Figures S6, S7 and S8) as well as the Cu(thd)$_2$ precursors (Figure S1 and S2) are detailed in the supporting information (Sections A and B).

3. Results and discussion

Materials deposited with an increasing number of cycles (160 and 250 cycles) were characterized by the means of scanning electron microscopy (SEM). As shown in Figure 1a and b, fairly homogeneous films with a good surface

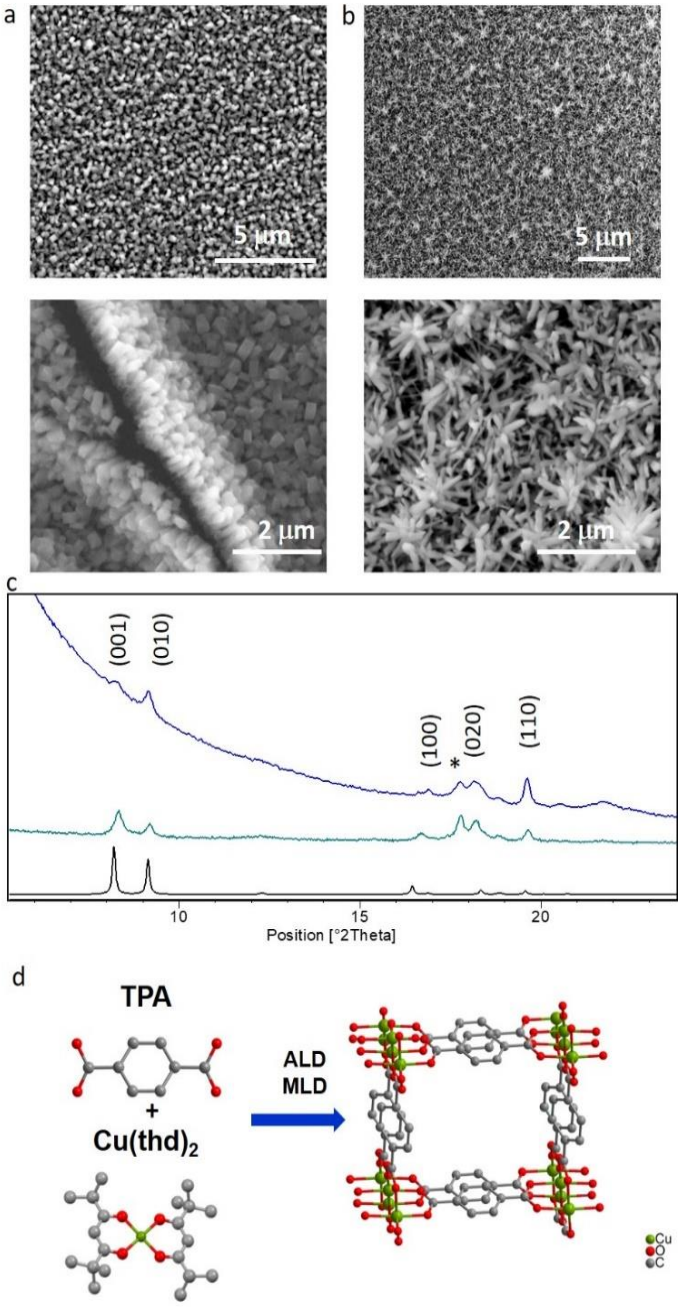

Figure 1: SEM images of the thin film obtained after 160 ALD/MLD cycles on Si (100), lower (top) and higher(bottom) magnifications (a), the film crack on the bottom image shows the oriented growth of the film. SEM images of the thin film obtained after 250 ALD/MLD cycles on Si (100), lower (top) and higher(bottom) magnifications (b). PXRD patterns of the films obtained after 160 cycles (blue) and after 250 cycles (teal), the calculated PXRD diagram for CuTPA (black), * corresponds to the free TPA (c), reaction scheme for the ALD/MLD of CuTPA (d)

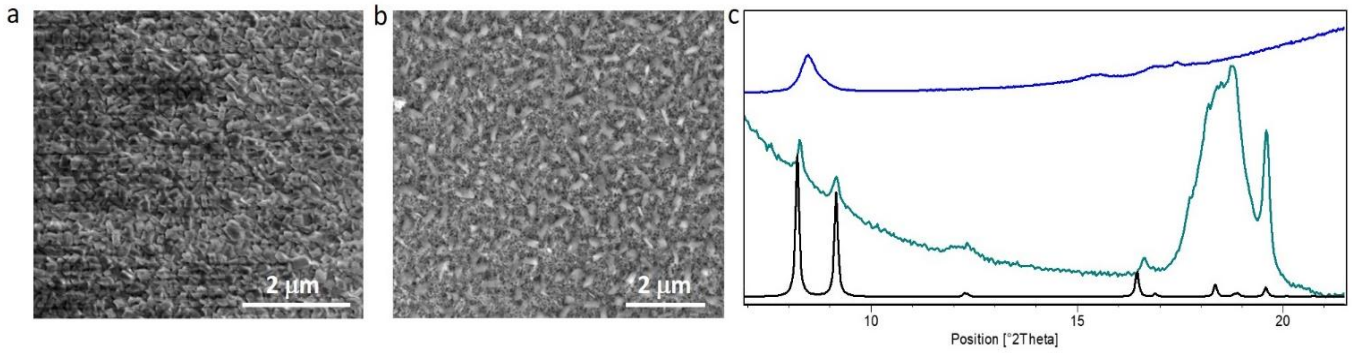

Figure 2: SEM image of the thin film deposited on sapphire, a-oriented substrate (a), SEM image of the thin film deposited on FTO (b), XRD patterns of the films deposited on sapphire (teal) and on FTO (blue) both films were deposited through 250 cycles, the calculated pattern for CuTPA is shown in black (c).

coverage were obtained (Figure S15a and b). The substrates were covered by well-defined rod-shaped crystallites of about 150 nm. For 160 cycles, an orientation of the crystallites perpendicular to the substrate is noticeable (Figure 1a), when increasing the number of cycles, crystallites start to grow on each other in a more isotropic way (Figure 1b). It can be noted here that the oriented growth at low number of cycles proceeds on amorphous surface of native oxide. Energy Dispersive Spectroscopy (EDS) analysis confirms the presence of Cu and C at the surface (Figure S17).

Structural analysis was performed by the means of XRD. The obtained films show good crystallinity as depicted in Figure 1c. Phase identification clearly demonstrates the formation of the triclinic 3-dimensional CuTPA framework[27], where the copper ions are solely connected by the carboxylate functions and form Cu-O chains that run in the same direction as the one-dimensional pores of ca 5.2 Å (Figure 1d). This clarifies the MOF phase obtained from the ALD/MLD process, which differs from the previously assigned paddle-wheel 2-dimensional structure. The observed 3D phase is in accordance with a solventless process, as no other linker than TPA is present in the Cu coordination sphere. The diffractograms in Figure 1c show some extra Bragg peaks that have been attributed to free TPA, probably due to its low volatility that prevents the total removal during the purge step. Attempts to avoid free TPA deposition using a shorter pulse and/or a lower temperature for this precursor (140 °C instead of 180 °C) led to a considerable loss of the film crystallinity that is evidenced by a considerable decrease of the diffraction peak intensity (Figure S12). To avoid the presence of unreacted TPA, a 5 µm filter gasket was implemented upstream from the reaction chamber and further studies were conducted with the standard parameters. More importantly, XRD patterns (Figure 1c) indicate that the film growth starts in an oriented manner, given the large relative intensities of the peaks corresponding to the (010) and (110) inter-reticular planes in the pattern corresponding to 160 cycles grown film. When further ALD/MLD cycles are implemented, the growth orientation becomes more random, as the relative intensities of Bragg peaks match closer to the calculated pattern for CuTPA. This points out that CuTPA growth first preferentially occurs perpendicular to the substrate along the [001] direction of the unit cell, meaning that the pores and the inorganic chains of the MOF run parallel to the substrate (Figure S10). After a certain film thickness, the ALD/MLD proceeds more isotropically. This analysis of XRD data is corroborated the SEM results (Figure 1a, b) discussed above. The reproducibility of the 3D phase film growth was checked by performing three

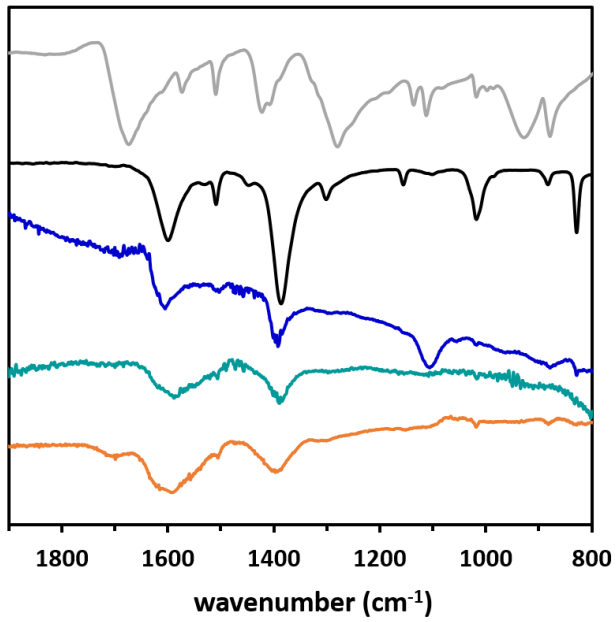

Figure 3: FTIR spectra of TPA (light grey), the bulk CuTPA (black), and CuTPA films grown on Si (100) with native oxide (blue), sapphire (teal) and FTO (orange).

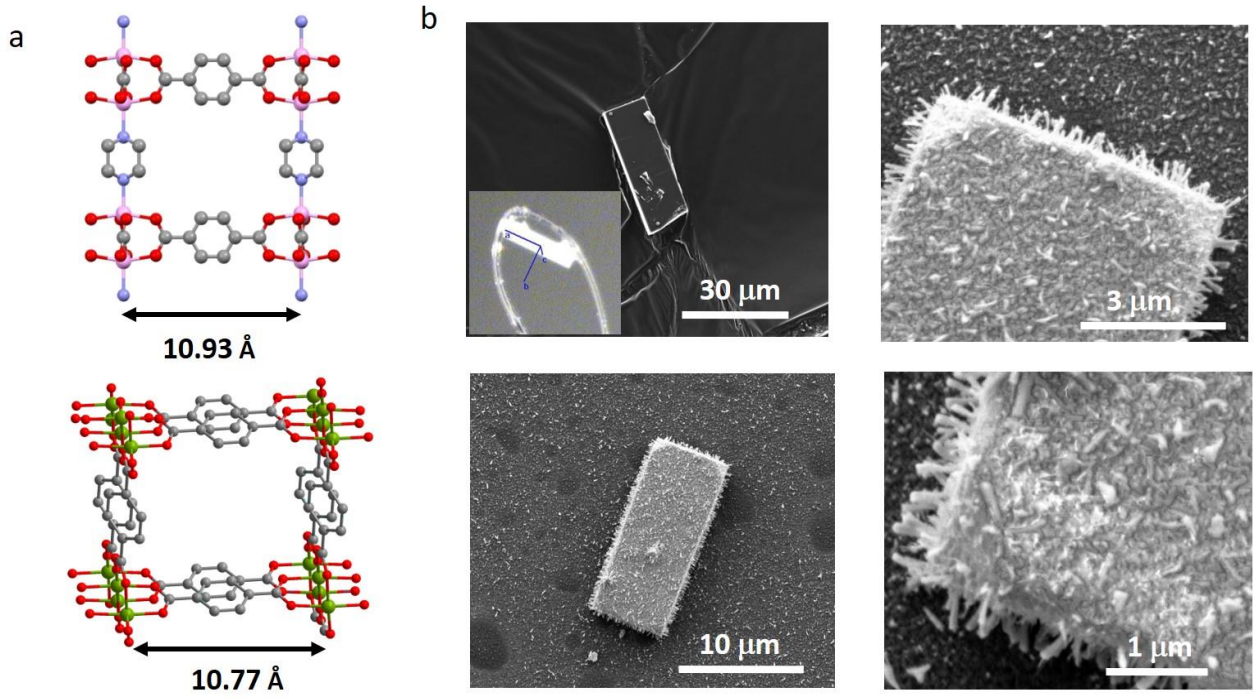

Figure 4: Representation of the DMOF-1 (left) and CuTPA(right) structures and the intermetallic distances (a), SEM images of DMOF-1 before (top left) and after 250 cycles of ALD/MLD of CuTPA.

times the deposition in the same conditions (Figure S11). MOF formation was further confirmed spectroscopically by FTIR analysis.

The spectra (Figure 3 and Figure S14) show vibrations bands 1590 cm^{-1} and 1390 cm^{-1} that are assigned to the asymmetric and symmetric vibrations of the carboxylate group, respectively. The Δ between these two frequencies (Δ=200 cm^{-1}) is characteristic of bidentate bridged carboxylate[28] and free TPA displays ν(C=O) and ν(C-O) bands at 1685 cm^{-1} and 1272 cm^{-1}, respectively (Figure 3). The obtained values match the ones observed for the bulk CuTPA that was synthesized in solution as a reference for this study (see SI, Figure S14a). It should be noted that the band at 1100 cm^{-1}, visible on the spectrum of CuTPA on Si wafer with native oxide, originates from the substrate (Figure S14b) and corresponds to the stretching band of Si-O-Si. The bulk MOF morphology can be described as a near-square shape assembly of platelets (Figure S5) while the ALD/MLD grown crystallites display a more elongated parallelepiped shape, indicative of their preferential c-axis orientation.

To check the adaptability of the process and investigate the impact of the starting surface, the film growth was then performed on crystalline substrates. Sapphire with c-plane surface orientation and FTO on glass were chosen, both kinds of substrates present oxide/hydroxide functionalities at their surface that are well suited for reacting with the metallic precursor. The ALD/MLD was implemented with the same parameters as for Si (100). The SEM data evidence that a crystalline film is obtained on both substrates, but the crystallite morphology differs (Figure 2a and b). Indeed, on the sapphire, a rather compact film formed of rod-like crystallites is observed when in the case of FTO, thinner and more dispersed crystallites are deposited. For both films, a good coverage is obtained (Figure S15c and d), Cu and C are detected by EDS (Figures S18, S19). XRD analysis (Figure 2c) reveals that the same CuTPA phase is clearly formed on the sapphire substrate when in the case of FTO the obtained pattern is ill-defined and does not allow accurate phase identification. This might be due to sparser film coverage. In all cases, FTIR analysis reveals the coordination of copper by the TPA linker (Figure 3).

Given the good adaptability of the process, we aimed to explore the heteroepitaxial MOF on MOF growth, using a single crystalline MOF as substrate. Assembling MOF on MOF heterostructures is of great interest to reach superstructures with tuned mechanical, adsorptive, and photophysical properties[29]. Up to date, core-shell[30–32], layered[33], complex ternary[34] and anisotropic[35] MOF on MOF superstructures were reported through solution-based synthesis. To the best of our knowledge, such superstructures are not reported through the use of the MOF growth in the vapour phase. DMOF-1 (Zn-TPA-DABCO) was chosen as the support because, in its structure, the intermetallic distances are very close to the ones in CuTPA (10.93 and 10.77 Å respectively, meaning a mismatch of ~1.5 % only, Figure 4a). Additionally, DMOF-1 is easily obtained as single crystals, offering a molecular material substrate with well-defined planar facets (Figure 4b and S8). From single crystal X-Ray diffraction analysis, the crystal orientation was determined, indicating that DMOF-1 grows along its 3 cell axes, with *a* axis as the preferential

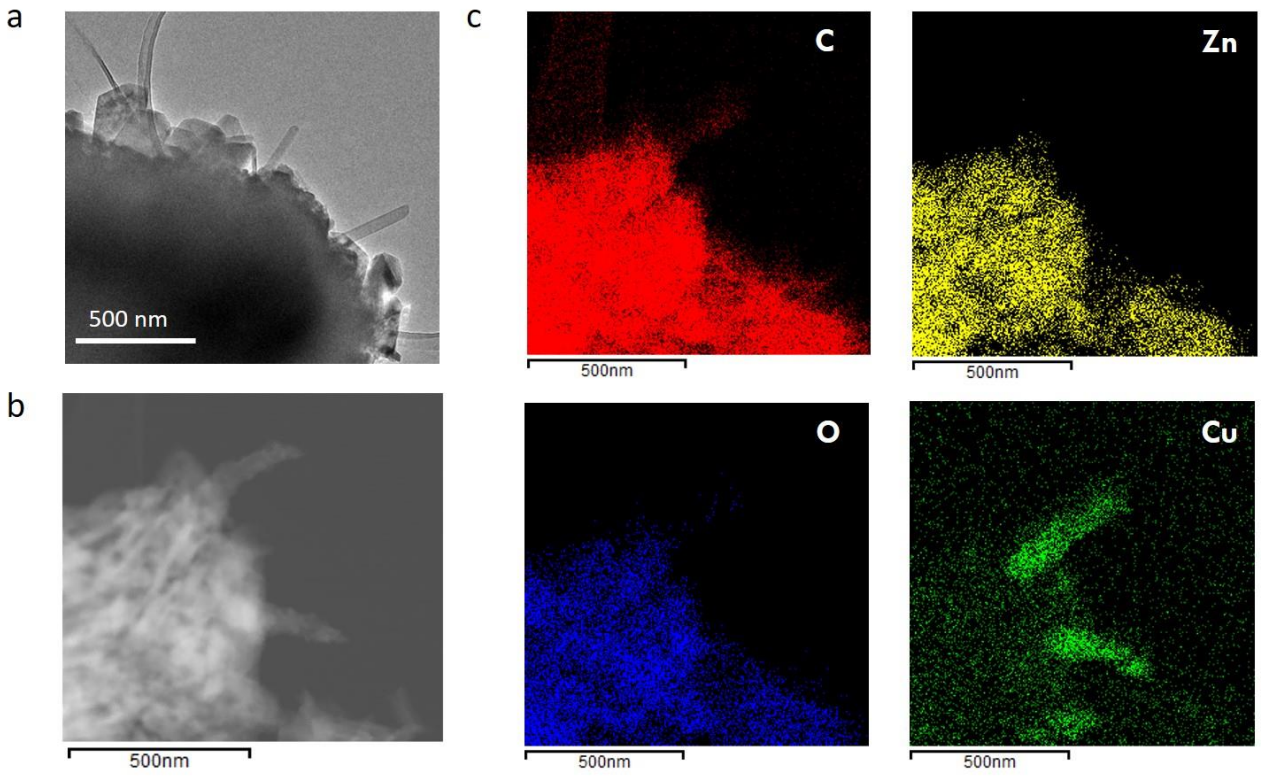

Figure 5: TEM image of DMOF-1 after 250 cycles of ALD/MLD of CuTPA (a), STEM image (b) and the corresponding elemental mapping performed by STEM-EDS (c)

direction (inset Figure 4 b). The pores width of DMOF-1 is insufficient for the diffusion of the $Cu(thd)_2$ precursor, therefore an on-surface only ALD/MLD reaction can be expected. DMOF-1 single crystals were dispersed onto the surface of Si (100) substrate and the ALD/MLD of CuTPA was performed. From the SEM analysis of the recovered sample, DMOF-1 surface is clearly altered as it appears covered by nanometric crystallites and a film deposition on the Si wafer is observed (Figure 4b). This way, a heterostructure resembling a core-shell topology is obtained through ALD/MLD implementation on the MOF surface.

More importantly, these crystallites are well-oriented perpendicular to the DMOF-1 surface all over the different facets (Figure 4b and S16), indicating that the ALD/MLD process allows directional growth on a structured three-dimensional substrate, with comparable intermetallic distances. EDS analysis indicates both the presence of Cu and Zn (Figure S20) on the crystal particles. To perform a spatial resolved analysis of the heterostructure, the CuTPA-coated crystals were transferred to an Au grid for transmission electron microscopy (TEM) analysis. The TEM image in Figure 5a shows thin crystallites sticking out of the DMOF-1 crystal. Elemental mapping was performed in STEM-EDS mode (Figure 5b and c), and clearly shows that Cu containing material is deposited on top of the Zn-based solid, demonstrating for the first time that a heterostructure is accessible using ALD/MLD on a MOF surface. In this set up, the deposition occurs both on the Si (100) and on DMOF-1 surfaces, which prevents thorough structural analysis of the heterostructure by X-Ray diffraction, nonetheless the obtained pattern displays Bragg peaks corresponding to the CuTPA phase (Figure S13).

4. Conclusions

In summary, this study clarifies and expands the scope of the ALD/MLD growth of crystalline MOF thin films. In particular, we demonstrate that the 3D CuTPA MOF films can be easily obtained through the vapour phase layer by layer growth and that this process is adaptable to different kinds of amorphous (Si with native oxide) or crystalline (sapphire, FTO) inorganic substrates. Importantly, for the first time an oriented MOF growth in vapour phase is detected and the orientation of the crystallites is determined. Notably, the directional MOF growth is also observed on the facets of DMOF-1 single crystals leading to an unprecedented core-shell material

by vapour phase synthesis. This proves the ability of the ALD/MLD technique to accomplish heteroepitaxial growth on structured hybrid materials with lattice matching topologies. Our results indicate that the ALD/MLD deserves to be further and wider advanced for the processing of hybrid materials and the development of functional heterojunctions.

Author contributions

Ben Gikonyo: investigation, validation
Fangbing Liu: investigation, validation
Siddhartha De: investigation
Catherine Journet: resources, data curation, visualization
Catherine Marichy: conceptualization, project administration, supervision, visualization, Writing-Original Draft, Writing - Review & Editing
Alexandra Fateeva: conceptualization, funding acquisition, resources, project administration, supervision, visualization, Writing-Original Draft, Writing - Review & Editing

Conflicts of interest

The authors declare that they have no competing financial interests or personal relationships that could have appeared to influence the work reported in this paper.

Acknowledgments

The authors gratefully acknowledge Pr. Jacques Jose for the technical help, the Centre Technologique des Microstructures of the University of Lyon for providing the electron microscopy facilities, the French Ministry of National Education, Research and Technology, the University Lyon 1 and the CNRS for financial support; this work was supported by the French National Research Agency grant (ANR-17-CE09-0029-01).

References

(1) Plutnar, J.; Pumera, M. Applications of Atomic Layer Deposition in Design of Systems for Energy Conversion. *SMALL* **2021**, *17* (39). https://doi.org/10.1002/smll.202102088.

(2) Tripathi, T.; Karppinen, M. Atomic Layer Deposition of P-Type Semiconducting Thin Films: A Review. *Adv. Mater. INTERFACES* **2017**, *4* (24). https://doi.org/10.1002/admi.201700300.

(3) Zhao, Y.; Zhang, L.; Liu, J.; Adair, K.; Zhao, F.; Sun, Y.; Wu, T.; Bi, X.; Amine, K.; Lu, J.; Sun, X. Atomic/Molecular Layer Deposition for Energy Storage and Conversion. *Chem. Soc. Rev.* **2021**, *50* (6), 3889–3956. https://doi.org/10.1039/d0cs00156b.

(4) Leskelä, M.; Mattinen, M.; Ritala, M. Review Article: Atomic Layer Deposition of Optoelectronic Materials. *J. Vac. Sci. Technol. B* **2019**, *37* (3), 030801. https://doi.org/10.1116/1.5083692.

(5) Johnson, R. W.; Hultqvist, A.; Bent, S. F. A Brief Review of Atomic Layer Deposition: From Fundamentals to Applications. *Mater. Today* **2014**, *17* (5), 236–246. https://doi.org/10.1016/j.mattod.2014.04.026.

(6) George, S. M. Atomic Layer Deposition: An Overview. *Chem. Rev.* **2010**, *110* (1), 111–131. https://doi.org/10.1021/cr900056b.

(7) Yoshimura, T.; Tatsuura, S.; Sotoyama, W. Polymer Films Formed with Monolayer Growth Steps by Molecular Layer Deposition. *Appl. Phys. Lett.* **1991**, *59* (4), 482–484. https://doi.org/10.1063/1.105415.

(8) Dameron, A. A.; Seghete, D.; Burton, B. B.; Davidson, S. D.; Cavanagh, A. S.; Bertrand, J. A.; George, S. M. Molecular Layer Deposition of Alucone Polymer Films Using Trimethylaluminum and Ethylene Glycol. *Chem. Mater.* **2008**, *20* (10), 3315–3326. https://doi.org/10.1021/cm7032977.

(9) Klepper, K. B.; Nilsen, O.; Fjellvåg, H. Deposition of Thin Films of Organic–Inorganic Hybrid Materials Based on Aromatic Carboxylic Acids by Atomic Layer Deposition. *Dalton Trans.* **2010**, *39* (48), 11628–11635. https://doi.org/10.1039/C0DT00817F.

(10) Ahvenniemi, E.; Karppinen, M. Atomic/Molecular Layer Deposition: A Direct Gas-Phase Route to Crystalline Metal–Organic Framework Thin Films. *Chem Commun* **2016**, *52* (6), 1139–1142. https://doi.org/10.1039/C5CC08538A.

(11) Ahvenniemi, E.; Karppinen, M. In Situ Atomic/Molecular Layer-by-Layer Deposition of Inorganic–Organic Coordination Network Thin Films from Gaseous Precursors. *Chem. Mater.* **2016**, *28* (17), 6260–6265. https://doi.org/10.1021/acs.chemmater.6b02496.

(12) Heiska, J.; Sorsa, O.; Kallio, T.; Karppinen, M. Benzenedisulfonic Acid as an ALD/MLD Building Block for Crystalline Metal-Organic Thin Films**. *Chem.- Eur. J.* **2021**, *27* (34), 8799–8803. https://doi.org/10.1002/chem.202100538.

(13) Multia, J.; Heiska, J.; Khayyami, A.; Karppinen, M. Electrochemically Active In Situ Crystalline Lithium-Organic Thin Films by ALD/MLD. *ACS Appl. Mater. INTERFACES* **2020**, *12* (37), 41557–41566. https://doi.org/10.1021/acsami.0c11822.

(14) Penttinen, J.; Nisula, M.; Karppinen, M. Atomic/Molecular Layer Deposition of s-Block Metal Carboxylate Coordination Network Thin Films. *Chem.-Eur. J.* **2017**, *23* (72), 18225–18231. https://doi.org/10.1002/chem.201703704.

(15) Tanskanen, A.; Karppinen, M. Iron-Terephthalate Coordination Network Thin Films Through In-Situ Atomic/Molecular Layer Deposition. *Sci. Rep.* **2018**, *8*. https://doi.org/10.1038/s41598-018-27124-7.

(16) Heiska, J.; Nisula, M.; Rautama, E.-L.; Karttunen, A. J.; Karppinen, M. Atomic/Molecular Layer Deposition and Electrochemical Performance of Dilithium 2-Aminoterephthalate. *Dalton Trans* **2020**, *49* (5), 1591–1599. https://doi.org/10.1039/C9DT04572D.

(17) Lausund, K. B.; Petrovic, V.; Nilsen, O. All-Gas-Phase Synthesis of Amino-Functionalized UiO-66 Thin Films. *Dalton Trans* **2017**, *46* (48), 16983–16992. https://doi.org/10.1039/C7DT03518G.

(18) Lausund, K. B.; Nilsen, O. All-Gas-Phase Synthesis of UiO-66 through Modulated Atomic Layer Deposition. *Nat. Commun.* **2016**, *7* (1), 13578. https://doi.org/10.1038/ncomms13578.

(19) Salmi, L. D.; Heikkilä, M. J.; Puukilainen, E.; Sajavaara, T.; Grosso, D.; Ritala, M. Studies on Atomic Layer Deposition of MOF-5 Thin Films. *Microporous Mesoporous Mater.* **2013**, *182*, 147–154. https://doi.org/10.1016/j.micromeso.2013.08.024.

(20) Salmi, L. D.; Heikkilä, M. J.; Vehkamäki, M.; Puukilainen, E.; Ritala, M.; Sajavaara, T. Studies on Atomic Layer Deposition of IRMOF-8 Thin Films. *J. Vac. Sci. Technol. A* **2015**, *33* (1), 01A121. https://doi.org/10.1116/1.4901455.

(21) Lausund, K. B.; Olsen, M. S.; Hansen, P.-A.; Valen, H.; Nilsen, O. MOF Thin Films with Bi-Aromatic Linkers Grown by Molecular Layer Deposition. *J Mater Chem A* **2020**, *8* (5), 2539–2548. https://doi.org/10.1039/C9TA09303F.

(22) Stassen, I.; De Vos, D.; Ameloot, R. Vapor-Phase Deposition and Modification of Metal–Organic Frameworks: State-of-the-Art and Future Directions. *Chem. – Eur. J.* **2016**, *22* (41), 14452–14460. https://doi.org/10.1002/chem.201601921.

(23) Su, P.; Tu, M.; Ameloot, R.; Li, W. Vapor-Phase Processing of Metal–Organic Frameworks. *Acc. Chem. Res.* **2022**, *55* (2), 186–196. https://doi.org/10.1021/acs.accounts.1c00600.

(24) Crivello, C.; Sevim, S.; Graniel, O.; Franco, C.; Pané, S.; Puigmartí-Luis, J.; Muñoz-Rojas, D. Advanced Technologies for the Fabrication of MOF Thin Films. *Mater. Horiz.* **2021**, *8* (1), 168–178. https://doi.org/10.1039/D0MH00898B.

(25) Sánchez-Sánchez, M.; Getachew, N.; Díaz, K.; Díaz-García, M.; Chebude, Y.; Díaz, I. Synthesis of Metal–Organic Frameworks in Water at Room Temperature: Salts as Linker Sources. *Green Chem* **2015**, *17* (3), 1500–1509. https://doi.org/10.1039/C4GC01861C.

(26) Ma, J.; Kalenak, A. P.; Wong-Foy, A. G.; Matzger, A. J. Rapid Guest Exchange and Ultra-Low Surface Tension Solvents Optimize Metal–Organic Framework Activation. *Angew. Chem. Int. Ed.* **2017**, *56* (46), 14618–14621. https://doi.org/10.1002/anie.201709187.

(27) Carson, C. G.; Brunnello, G.; Lee, S. G.; Jang, S. S.; Gerhardt, R. A.; Tannenbaum, R. Structure Solution from Powder Diffraction of Copper 1,4-Benzenedicarboxylate. *Eur. J. Inorg. Chem.* **2014**, *2014* (12), 2140–2145. https://doi.org/10.1002/ejic.201301543.

(28) Tan, K.; Nijem, N.; Canepa, P.; Gong, Q.; Li, J.; Thonhauser, T.; Chabal, Y. J. Stability and Hydrolyzation of Metal Organic Frameworks with Paddle-Wheel SBUs upon Hydration. *Chem. Mater.* **2012**, *24* (16), 3153–3167. https://doi.org/10.1021/cm301427w.

(29) Haldar, R.; Wöll, C. Hierarchical Assemblies of Molecular Frameworks—MOF-on-MOF Epitaxial Heterostructures. *Nano Res.* **2021**, *14* (2), 355–368. https://doi.org/10.1007/s12274-020-2953-z.

(30) Furukawa, S.; Hirai, K.; Nakagawa, K.; Takashima, Y.; Matsuda, R.; Tsuruoka, T.; Kondo, M.; Haruki, R.; Tanaka, D.; Sakamoto, H.; Shimomura, S.; Sakata, O.; Kitagawa, S. Heterogeneously Hybridized Porous Coordination Polymer Crystals: Fabrication of Heterometallic Core–Shell Single Crystals with an In-Plane Rotational Epitaxial Relationship. *Angew. Chem. Int. Ed.* **2009**, *48* (10), 1766–1770. https://doi.org/10.1002/anie.200804836.

(31) Faustini, M.; Kim, J.; Jeong, G.-Y.; Kim, J. Y.; Moon, H. R.; Ahn, W.-S.; Kim, D.-P. Microfluidic Approach toward Continuous and Ultrafast Synthesis of Metal–Organic Framework Crystals and Hetero Structures in Confined Microdroplets. *J. Am. Chem. Soc.* **2013**, *135* (39), 14619–14626. https://doi.org/10.1021/ja4039642.

(32) Yu, D.; Song, Q.; Cui, J.; Zheng, H.; Zhang, Y.; Liu, J.; Lv, J.; Xu, T.; Wu, Y. Designing Core–Shell Metal–Organic Framework Hybrids: Toward High-Efficiency Electrochemical Potassium Storage. *J. Mater. Chem. A* **2021**, *9* (46), 26181–26188. https://doi.org/10.1039/D1TA08215A.

(33) Ikigaki, K.; Okada, K.; Tokudome, Y.; Toyao, T.; Falcaro, P.; Doonan, C. J.; Takahashi, M. MOF-on-MOF: Oriented Growth of Multiple Layered Thin Films of Metal–Organic Frameworks. *Angew. Chem. Int. Ed.* **2019**, *58* (21), 6886–6890. https://doi.org/10.1002/anie.201901707.

(34) Liu, C.; Sun, Q.; Lin, L.; Wang, J.; Zhang, C.; Xia, C.; Bao, T.; Wan, J.; Huang, R.; Zou, J.; Yu, C. Ternary MOF-on-MOF Heterostructures with Controllable Architectural and Compositional Complexity via Multiple Selective Assembly. *Nat. Commun.* **2020**, *11* (1), 4971. https://doi.org/10.1038/s41467-020-18776-z.

(35) Lee, G.; Lee, S.; Oh, S.; Kim, D.; Oh, M. Tip-To-Middle Anisotropic MOF-On-MOF Growth with a Structural Adjustment. *J. Am. Chem. Soc.* **2020**, *142* (6), 3042–3049. https://doi.org/10.1021/jacs.9b12193.